Acta Crystallographica Section D
Biological Crystallography
ISSN 0907-4449

On the application of molecular-dynamics simulations to validate thermal parameters and to optimize TLS-group selection for macromolecular refinement

Nicholas M. Glykos

Department of Molecular Biology and Genetics, Democritus University of Thrace, Dimitras 19, 68100 Alexandroupolis, Greece

Correspondence e-mail: glykos@mbg.duth.gr

Received 7 March 2007
Accepted 27 March 2007

PDB Reference: RM6 Rop deletion mutant, 1qx8, r1qx8sf.

Comparison of crystallographically determined and molecular dynamics simulation-derived parameters for a small (26 kDa) homotetrameric four-α-helical bundle protein revealed an unexpected pattern of similarities and differences between experiment and simulation. On one hand, the protein structure *per se* is exceptionally well preserved during the simulations, with a root-mean-square deviation between the C^{α} atoms of the crystal structure and the simulation-derived average structures of only 0.58 Å, which is not very different from the expected coordinate error of the experimentally determined structure. On the other hand, comparison of the temperature factors showed a large discrepancy, with the experimental *B* factors being approximately three times higher than the simulation-derived *B* factors. Closer examination of this discrepancy appears to validate the molecular-dynamics prediction and to implicate as its source static disorder at the crystalline state, as indicated by the strong diffuse scattering and pronounced anisotropy of the diffraction pattern of the protein crystals. *A posteriori* re-refinement of the structure using a new TLS parameterization scheme based on the results obtained from the simulations led to a further reduction of the *R* factor and the free *R* value by 0.4% and 0.8%, respectively, indicating that molecular-dynamics simulations have matured to the point that they can be used to aid the selection of TLS groups for macromolecular refinement.

1. Introduction

Molecular-dynamics simulations have traditionally been treated with caution, if not skepticism, by crystallographers. This is rightly so: the force fields upon which molecular dynamics are based represent empirical models, the validity of which (for the problem in hand) must always be ascertained. The aforementioned skepticism has been reinforced in the past by the lack of stability of the molecular-dynamics trajectories, especially in the case of highly charged macromolecules such as nucleic acids (Cheatham & Young, 2001). The implementation over the past decade of fast full electrostatics methods, together with the steady increase in computational power available to laboratories (mainly owing to the introduction of Beowulf-type computer clusters), has transformed the field of macromolecular simulation (Schlick, 2001). Current-generation molecular-dynamics protocols and programs give trajectories that are well behaved and stable for simulations lasting from tens to hundreds of nanoseconds. The

availability of stable trajectories, together with the apparent convergence of the various force fields (Rueda *et al.*, 2007), has shifted interest to the question of whether the molecular-dynamics simulations have predictive power; that is, whether they can lead to experimentally verifiable predictions. This question is of special interest for the case of crystallographically determined structures: the availability of dependable molecular-dynamics protocols would provide a route for establishing the long-sought connection between a static (time-and-space averaged) structure and its dynamical properties.

Here, results are presented of a comparison between the crystallographically determined and simulation-derived parameters of a small protein and it is shown that molecular dynamics have sufficient predictive power to guide the selection of TLS groups for macromolecular refinement.

2. Computational procedures

2.1. Crystallographic data

The protein used in this study is RM6, a small (26 kDa) homotetrameric four-α-helical bundle corresponding to a five-residue deletion mutant of the repressor of primer (Rop) protein. A detailed account of the crystallization, data collection and crystallographic structure determination of RM6 is given in Papanikolau *et al.* (2004) and Glykos *et al.* (2006). In summary, the RM6 crystals belong to space group $C2$, with unit-cell parameters $a = 54.5$, $b = 42.5$, $c = 51.7$ Å, $\beta = 104.7^\circ$, and contain the equivalent of half a bundle (two monomers) per asymmetric unit (with the whole bundle being formed through the application of a crystallographic twofold axis). Crystallographic data were collected at room temperature on a MAR Research image-plate detector. Indexing and integration were performed using the *HKL* system (Otwinowski & Minor, 1997) and resulted in data that were useful to 2.0 Å with an overall $R_{\rm sym}$ of 6.6% (31.2% in the last resolution shell), an overall completeness of 95.3% (76.0% in the last shell) and an average redundancy of 3.8 (2.6 in the last shell). The structure was determined using molecular replacement. Initial refinement was performed using a combination of torsion-angle dynamics, simulated annealing and addition of the most well ordered water molecules using *CNS* (Brünger *et al.*, 1998) and *Xfit* (from the *XtalView* suite of programs; McRee, 1992). This procedure converged to a mostly complete model with an R factor of 0.235 and a free R value of 0.267 for all data. The refinement was completed with successive rounds of maximum-likelihood refinement using the program *REFMAC* (Murshudov *et al.*, 1997), interspersed with the addition of further water molecules and fitting of discretely disordered residues. The final refinement step included one round of TLS refinement (Schomaker & Trueblood, 1998) using *REFMAC* and led to a final model with an R factor of 0.190 and a free R value of 0.212. The TLS refinement procedure was performed using only one set of TLS parameters per helix (*i.e.* each helix was treated as one rigid body). All other crystallographic calculations were performed using programs from the *CCP*4 suite (Collaborative Computational Project, Number 4, 1994) and *X-PLOR* (Brünger, 1992).

2.2. Molecular-dynamics simulations

An extensive set of molecular-dynamics simulations was performed using periodic boundary conditions with explicit representation of water and a full treatment of the electrostatics. The dynamics of six independent trajectories amounting to a total simulation time of 54.4 ns were followed. A detailed description of the simulation protocol is as follows. Starting from the crystallographically determined coordinates of RM6, missing side-chain and H atoms were built using the program *PSFGEN* from the *NAMD* distribution (Kale *et al.*, 1999) and assuming an acidic pH (with the histidines fully protonated) to match the pH of the crystallization mother liquor. Three different explicit solvation systems were prepared, each with a successively larger volume (and thus number of water molecules). This multiplicity of hydration systems allowed us to confirm that the electrostatic interaction between the periodic images of RM6 (arising from the periodic boundary conditions used for the simulations) does not significantly alter the dynamics of individual RM6 molecules.

The three hydration systems used in our simulations are (i) a relatively tight hexagonal cell comprising 4675 pre-equilibrated TIP3 water molecules (Jorgensen *et al.*, 1983) with a shortest (initial) solute–solute distance of 20 Å, (ii) a larger hexagonal cell comprising 7966 pre-equilibrated TIP3 water molecules with a shortest (initial) solute–solute distance of 30 Å and (iii) a truncated octahedral cell with a shortest dimension of 89 Å (which is approximately 8 Å longer than the longest dimension of the RM6 bundle) comprising 10 321 pre-equilibrated TIP3 water molecules. For all three systems the crystallographically determined waters were retained, while those water molecules lying closer than 1.8 Å from the protein surface (or the crystallographic waters) were removed. The final systems comprised 3216 protein atoms and 14 025, 23 898 or 30 963 water atoms depending on the periodic boundary cell used (see above). The net charge of the solute was neutralized through the addition of sodium and chloride ions to a final concentration of 100 mM (one sodium and three choride ions for the tight hexagonal cell, three and five, respectively, for the large hexagonal cell and five and seven, respectively, for the octahedral cell).

The molecular-dynamics simulations were performed with the program *NAMD* using the CHARMM27 force field (MacKerell *et al.*, 1998) as follows. The systems were first energy-minimized for 2000 conjugate-gradient steps with the positions of the backbone atoms fixed and then for another 2000 steps without positional restraints. They were then slowly heated to a final temperature of 320 K (with a temperature step $\Delta T = 20$ K) over a period of 66 ps with the positions of the C^α atoms harmonically restrained about their energy-minimized positions. Subsequently, the systems were equilibrated for 200 ps under NpT conditions without any restraints. This was followed by the production NpT runs with the temperature and pressure controlled using the Nosé-Hoover

Langevin dynamics and Langevin piston barostat control methods as implemented by the *NAMD* program [and maintained at 320 K and 1 atm (101.325 kPa)]. For the tight hexagonal cell system three independent production runs were performed, giving a total simulation time of 34.2 ns (with each run lasting for 7.6, 14.2 and 12.5 ns, respectively). For the large hexagonal cell, one production run was performed which lasted 12.7 ns. Finally, for the truncated octahedral cell the dynamics were followed for two production runs of lengths 4.6 and 2.8 ns, respectively. All production runs were performed using the impulse Verlet-I multiple timestep integration algorithm as implemented by *NAMD*. The inner timestep was 2 fs, short-range nonbonded interactions were calculated every two steps and long-range electrostatics interactions every four time steps using the particle-mesh Ewald method (Darden *et al.*, 1993). A cutoff for the van der Waals interactions was applied through a switching function and *SHAKE* was used to restrain all bonds involving H atoms. Trajectories were obtained by saving the atomic coordinates of the whole system every 0.4 ps.

Calculation of the isotropic displacement parameters from the molecular-dynamics trajectories (Fig. 4) was based on the atomic mean-squared displacements over the length of the trajectories using the equation (Stocker & van Gunsteren, 2006; García *et al.*, 1997)

$$B_i = \frac{8\pi^2}{3}\langle(\mathbf{r}_i - \langle\mathbf{r}_i\rangle)^2\rangle,$$

where $\mathbf{r}_i$ is the positional vector of the atom i and the angled brackets denote time averaging over the length of a trajectory.

For the analysis of the resulting trajectories, the programs *X-PLOR* (Brünger, 1992), *GROMACS* (Lindahl *et al.*, 2001), *VMD* (Humphrey *et al.*, 1996) and *Carma* (Glykos, 2006) were used.

Figures were prepared using the programs *VMD* (Humphrey *et al.*, 1996) and *RASTER3D* (Merritt & Bacon, 1997).

3. Results

A schematic diagram of the RM6 crystal structure together with part of a typical diffraction pattern recorded from its crystals is shown in Fig. 1 (see §2.1 for details of the crystallographic procedures). RM6 is a homotetrameric, all-antiparallel, left-handed four-α-helical bundle. Each monomer (of the tetramer) corresponds to one Rop polypeptide chain and forms a continuous α-helix (instead of a helix–turn–helix motif as in wild-type Rop; see Glykos *et al.*, 2006). The helices twist around one another and form a four-stranded left-handed coiled coil. The crystallographically determined

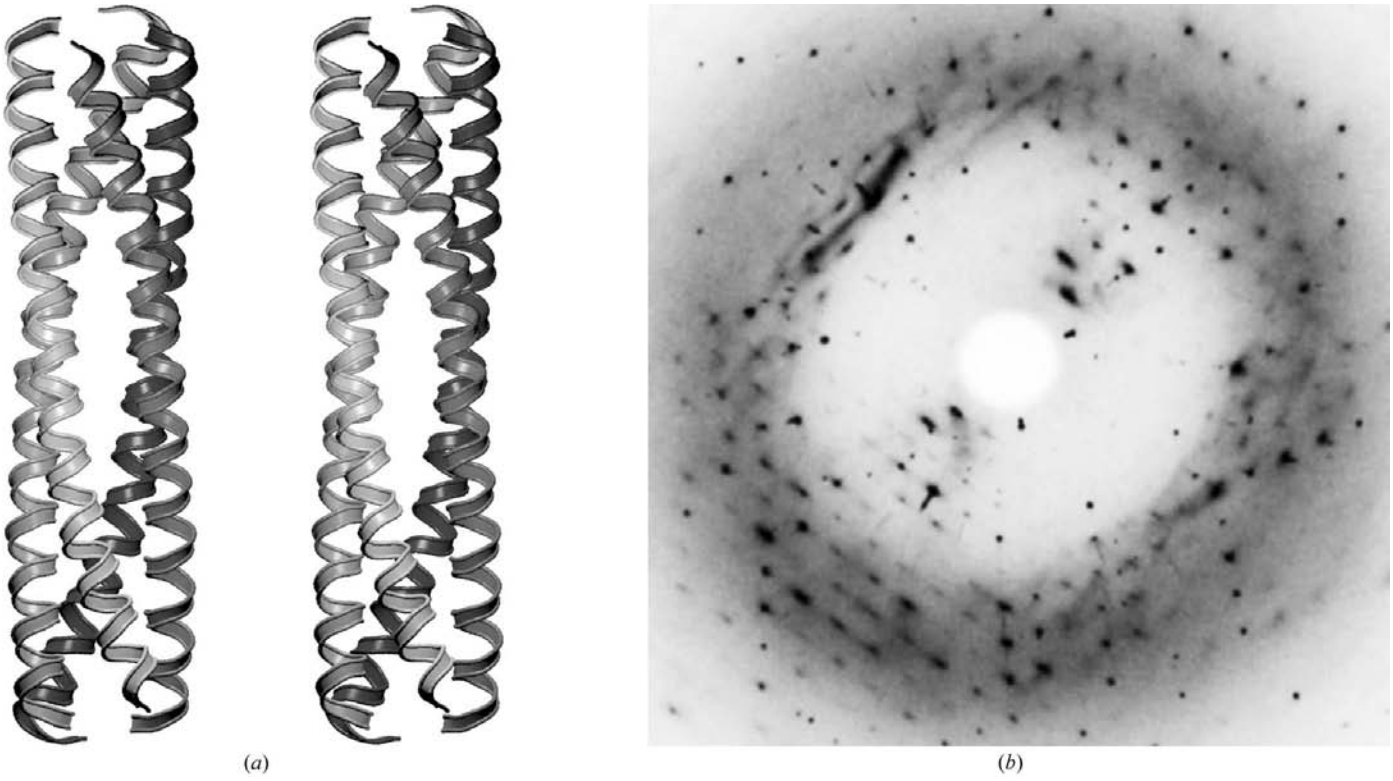

Figure 1
Schematic stereodiagram of the RM6 crystal structure (*a*) and a portion of a typical diffraction image recorded from its crystals (*b*). The structure diagram shows a complete four-α-helical bundle with the intramolecular twofold symmetry axis (which coincides with a crystallographic twofold axis) being approximately perpendicular to the plane of the page and passing through the centre of the molecule. In the diffraction image, notice the strong diffuse scattering and the asymmetric shape of the reflections.

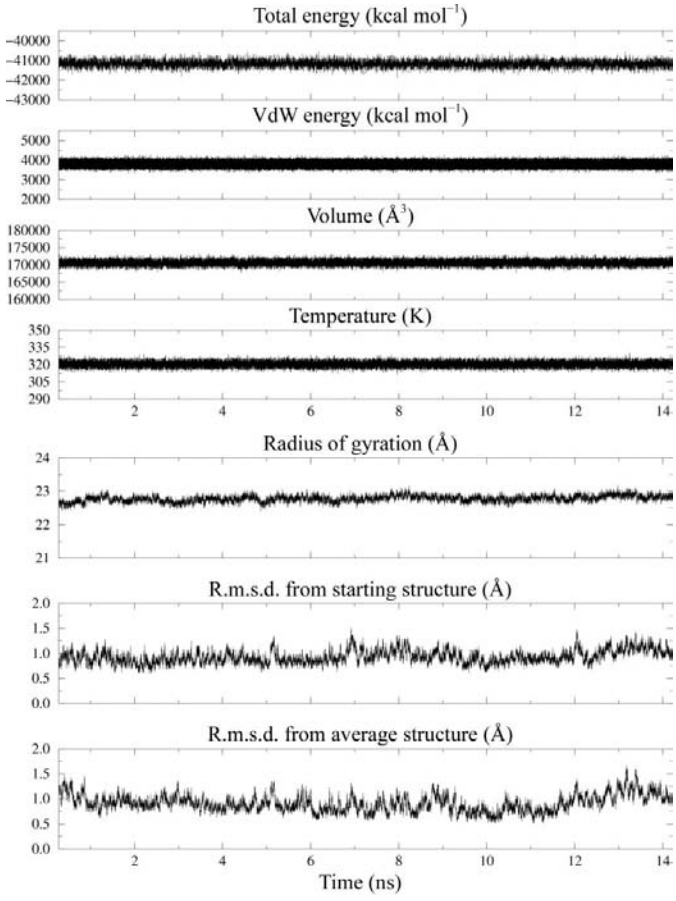

Figure 2
The top four graphs show the evolution of a selection of state variables for the longest continuous molecular-dynamics trajectory. The lower three graphs show the evolution of the radius of gyration and of the r.m.s. deviation from the starting and trajectory-average structures for the protein component. 1 kcal = 4.186 kJ.

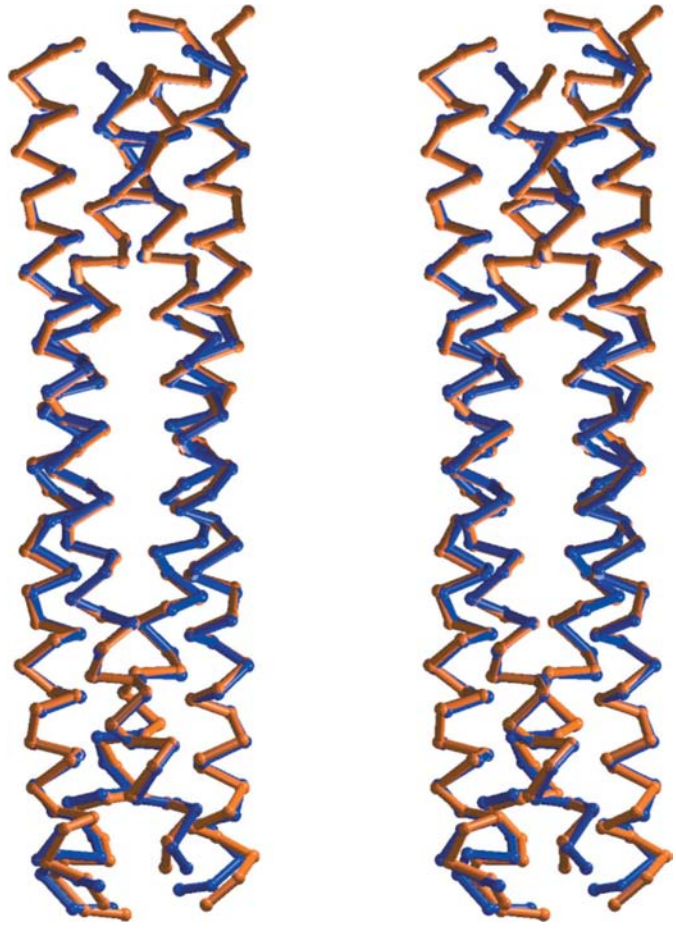

Figure 3
Stereodiagram of a superposition of the RM6 crystal structure (blue) and the molecular-dynamics-derived average structure (orange) from the longest continuous trajectory. The view is along the intramolecular twofold axis and only C^{α} atoms are shown.

coordinates of the four monomers are not independent: the complete bundle is formed through the application of a crystallographic twofold symmetry axis. While thermodynamic and kinetic characterization of RM6 has shown it to be a hyperstable homotetramer [with a melting temperature of about 373 K (100°C); Lassalle *et al.*, 1998], the thermal parameters of our crystal structure indicated a rather mobile molecule with average main-chain *B* factors of about 54 Å^2. This discrepancy between the thermodynamic parameters obtained from solution studies on one hand and the *B* factors of the crystal structure on the other led us to an attempt to characterize the mobility of RM6 using equilibrium molecular-dynamics simulations[1] (see §2.2 for details of the simulation protocols).

All simulations were very stable with respect to both their state variables and the structure of the solute. As an example, Fig. 2 shows the typical results obtained from our longest continuous trajectory (unless otherwise noted, all molecular-dynamics-related results reported in this communication are representative of all trajectories and not just the one used for illustration purposes). The top four graphs in this figure show that the depicted thermodynamic variables are stable throughout the length of the simulation, as expected from a fully equilibrated system. The lower three graphs show the evolution of protein structure-dependent quantities such as the radius of gyration and the r.m.s. deviation from the starting and trajectory-average structures. Not only are the trajectory-derived structures very similar to each other, they are also in excellent agreement with the crystal structure: the C^{α} r.m.s. deviations between the crystal structure and the average structures from our six trajectories are 0.582, 0.591, 0.758, 0.503, 0.596 and 0.468 Å, which are not very different from the expected error of the crystal structure. Furthermore, as shown by Fig. 3, the deviations between the crystal and trajectory-derived structures are not uniformly distributed throughout the molecule, but are mostly located at the helix termini, which are highly mobile (see below). In summary, the experimental

[1] Note that what we attempt to characterize are the dynamics of the protein *per se* and not the dynamics of the correlated protein motion in the crystalline state. The amount of diffuse scattering seen in Fig. 1 clearly indicates that the RM6 crystals could have been the subject of a molecular-dynamics study in the crystalline state as described by Micu & Smith (1995), but such a study is outside the scope of this communication.

and simulation-derived structures are in excellent agreement with respect to the positional parameters of the structure.

Turning our attention to the thermal parameters, Fig. 4 shows a comparison of the experimental and simulation-derived atomic temperature factors (noting that all simulations were performed at 320 K). In contrast to general experience and expectations (see, for example, SI-Fig. 10 from Rueda *et al.*, 2007), the simulation-derived *B* factors are approximately three times lower than the experimental ones. However, it is only the absolute magnitudes that differ and not their pattern of variation across the polypeptide chains: both experiment and simulation show that the termini of the four helices are highly mobile and that there is a noticeable increase of mobility in the central part of all four helices. To quantify this statement, the linear correlation coefficient between the crystallographic and the average simulation-derived *B* factors was calculated and found to be as high as 0.83. Further testimony to the underlying similarity between experiment and simulation comes from a comparison of the simulation-derived thermal parameters of pairs of helices that are related by the intramolecular symmetry and pairs of helices that are not[2]. The linear correlation coefficient between the *B* factors of symmetry-related helices stands at a hefty 0.98, which is significantly higher than the value of 0.82 corresponding to the non-symmetry-related helices (the values quoted are averages over all possible pairs). What this implies is that the simulation preserves molecular symmetry even in the absence of crystallographic symmetry restraints. It would thus appear that experiment and simulation are in excellent agreement with each other on all aspects of the thermal parameters of the protein, except the scale of the atomic temperature factors. The solution studies of Lassalle *et al.* (1998), together with the strong diffuse scattering and pronounced anisotropy of the diffraction patterns of the RM6 crystals (see Fig. 1), strongly suggest that the relatively high values of the crystallographically determined *B* factors are not the result of protein mobility but of static disorder in the crystalline state.

In an attempt to further validate the simulation-derived predictions concerning the thermal parameters of the protein, it was decided to re-examine the TLS-group selection used for the final stage of the crystallographic refinement. The reason for undertaking these calculations was that they were perceived to be an opportunity to experimentally verify the simulation results. As mentioned in §2.1, the TLS model for the deposited PDB structure treated each helix (monomer) as an independent group. If analysis of the molecular-dynamics simulations suggested a different para-

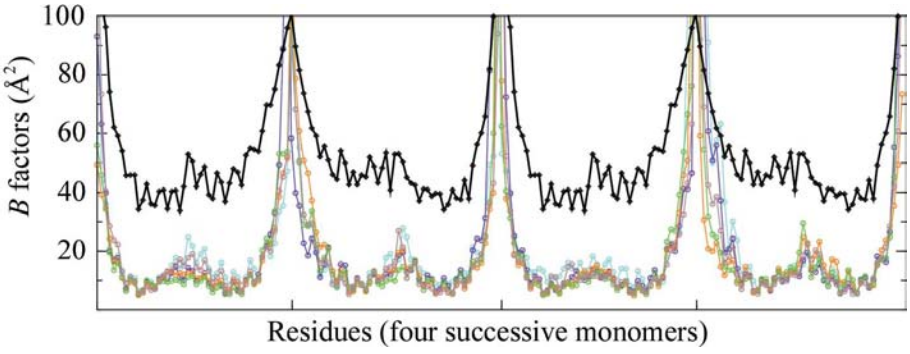

Figure 4
Comparison of the crystallographic (upper black curve) and simulation-derived *B* factors (lower curves) for all C^{α} atoms of the tetramer. The horizontal axis corresponds to successive residues of all four monomers. The limits of individual monomers are indicated by tick marks. Owing to crystallographic symmetry, the unique part of the experimental curve is that corresponding to the first two monomers.

[2] Such a comparison is possible owing to the absence of crystallographic symmetry from the molecular-dynamics simulations: the parameters of the four monomers are no longer constrained to be identical in pairs.

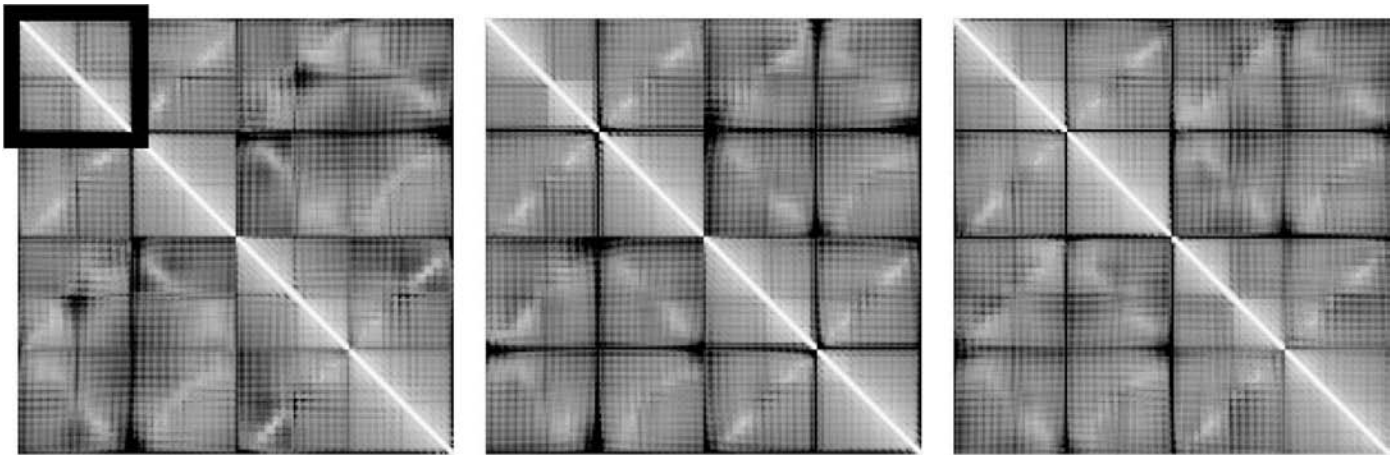

Figure 5
Grayscale representation of r.m.s. deviations of the $C^{\alpha}-C^{\alpha}$ distances from their average values during three molecular-dynamics simulations (with the middle graph corresponding to the longest continuous trajectory discussed in Figs. 2, 3 and 6). In all three diagrams, the horizontal and vertical axes correspond to successive residues of the tetramer, with successive monomers being clearly delineated owing to the presence of highly mobile termini. For the first diagram, the area corresponding to one helix is shown in a box. The contrast for all diagrams ranges from 0 Å (white) to 1 Å (black).

meterization, then it should be possible to experimentally verify the simulation-derived predictions by repeating the TLS refinement step (using the simulation-derived groups) while monitoring the free R value. Before presenting the results of these calculations, it is probably necessary to note that there are several possible pitfalls in the suggested procedure. The first is that TLS parameters can absorb errors in the modelling of the crystallographic data, especially their anisotropic scaling. The result would be an improvement in the values of global statistics such as the free R factor, but, unfortunately, not for the reasons envisioned. A second more subtle problem is that TLS parameters attempt to model the motion of rigid bodies, irrespectively of the exact dynamics involved (for example, whether the atomic motion is correlated or anticorrelated). From this perspective, a reduction of the free R value would validate not just the simulation-derived model, but a multitude of other models with completely different dynamics. The implication of this analysis is that the results presented below can only be interpreted as suggestive.

Several different approaches have been followed in an attempt to answer the question of how best to define groups suitable for TLS refinement based on the molecular-dynamics trajectories. The most simple-minded approach is based on the calculation of the average $C^{\alpha}-C^{\alpha}$ distances (during a trajectory) followed by calculation of the r.m.s. deviation of these distances from their average. Parts of the structure that exhibit low r.m.s. deviations between their C^{α} atoms can be taken to represent a rigid body. An example of such a calculation is shown in Fig. 5 for the three longest RM6 trajectories. Judging from the appearance of these diagrams (especially the parts corresponding to the intrahelix vectors of the first and third helix), it can be argued that a sensible arrangement would be to treat each helix as two groups, with the N-terminal group being somewhat longer than the C-terminal group. The problem with these $C^{\alpha}-C^{\alpha}$ r.m.s.d. maps is that they completely ignore the wealth of dynamical information present in the trajectories. A pictorial indication of the amount of information that is present in the trajectories but is missing from these $C^{\alpha}-C^{\alpha}$ r.m.s.d. maps is shown in Fig. 6, which depicts the average structure of RM6 (from the longest trajectory) using the thermal anisotropic ellipsoids calculated from the motion of the backbone plus C^{β} atoms during the simulation. The presence of obvious and distinct correlations in the direction of the major ellipsoid axes for the atoms of the middle part of the structure immediately suggests a different tripartite organization for each of the helices. This division of each helix in three groups (with a rather longer middle group) is clearly supported by the variance–covariance matrices obtained from the three longest trajectories and shown in Fig. 7: a constant and distinct tripartite pattern of correlated and anticorrelated motion connecting the middle part of each helix with its termini is evident. The limits (in terms of residues) of the three groups have been determined from these diagrams to be the following: from the N-terminus up to and including residue 16 (first group), from residue 17 up to and including residue 37 (second group) and from residue 38 to the C-terminus (third group). Consistent with the indications obtained from the variance–covariance matrices are the results from a principal-component analysis of the molecular-dynamics trajectories[3] (Amadei *et al.*, 1993; Ichiye & Karplus, 1991). To give an illustrated example, Fig. 8 shows the C^{α} motion corresponding to the first two principal components of the longest trajectory: the treatment of each helix in terms of three rigid groups is consistent both with the first component

Table 1
Overlap between eigenvector subspaces for the three longest molecular-dynamics trajectories.

The overlap between subspaces defined by two sets **v** and **w** of n eigenvectors is defined as $\text{overlap}(\mathbf{v}, \mathbf{w}) = (1/n)\sum_{i=1}^{n}\sum_{j=1}^{n}(\mathbf{v}_i \cdot \mathbf{w}_j)^2$. Overlap values range from zero (signifying no convergence of the corresponding subspaces) to one (for full overlap of the subspaces).

	No. of eigenvectors			
	1	2	3	4
Sim1–Sim2	0.3482	0.4340	0.8220	0.6596
Sim1–Sim3	0.4465	0.3993	0.8420	0.7366
Sim2–Sim3	0.0595	0.4623	0.7973	0.6610

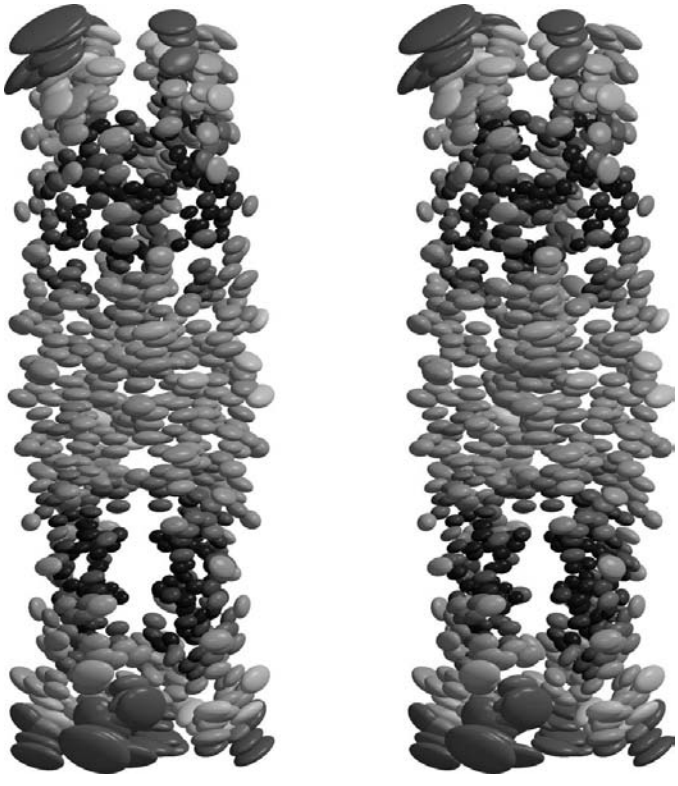

Figure 6
Stereodiagram of the average structure of RM6 from the longest molecular-dynamics trajectory using the thermal anisotropic ellipsoids calculated from the motion of the backbone plus C^{β} atoms during the simulation. The isosurfaces of the ellipsoids are drawn at the 0.90 probability level. The greyscale gradient used in this image corresponds to the values of the equivalent isotropic temperature factors of the atoms in the range 8–30 Å^2.

[3] The consistency between these two approaches is not surprising given that the principal components have been determined from the diagonalization of these same variance–covariance matrices.

Table 2
Comparison between the *R* factors and the free *R* values of the four different TLS models examined.

See text for details.

	R factor (%)	Free *R* value (%)
One group per helix	19.0	21.2
Two groups per helix	18.7	21.0
Three equal-length groups per helix	18.6	21.2
Three MD-derived groups per helix	18.6	20.4

(in which case, the middle group contributes significantly to the overall motion) and the second component (with contributions mainly from the terminal groups). An additional advantage of performing a principal-component analysis of the trajectories is that it allows the extraction of a quantitative answer to the ever-present question of whether molecular motion has been sufficiently sampled during the simulations (Lange & Grubmüller, 2006; Grossfield *et al.*, 2007). Demonstration of sufficient sampling of the molecular-dynamics trajectories is necessary not just for the principal-component analysis, but also for validating the results extracted from direct examination of the variance–covariance matrices. Of the many measures available for quantifying the convergence of sampling, Table 1 shows the values of overlap between eigenvector-defined subspaces derived from the three longest trajectories. As can be seen from this table, the subspaces defined by the three eigenvectors corresponding to the three largest eigenvalues have almost fully converged, increasing the confidence in the analysis presented above.

Based on the results presented in the previous paragraph, we compared four different TLS parameterization models with respect to the final *R* and free *R* values produced by re-refining the RM6 structure. The first TLS model comprises one group per helix and is identical to that used for the deposited PDB structure (1qx8). The second scheme implements the two-groups-per-helix model suggested from the examination of the $C^{\alpha}-C^{\alpha}$ r.m.s.d. maps. The third model consists of three groups per helix, but instead of using the molecular-dynamics-derived groups, three approximately equal-sized groups were used (N-terminus to residue 20,

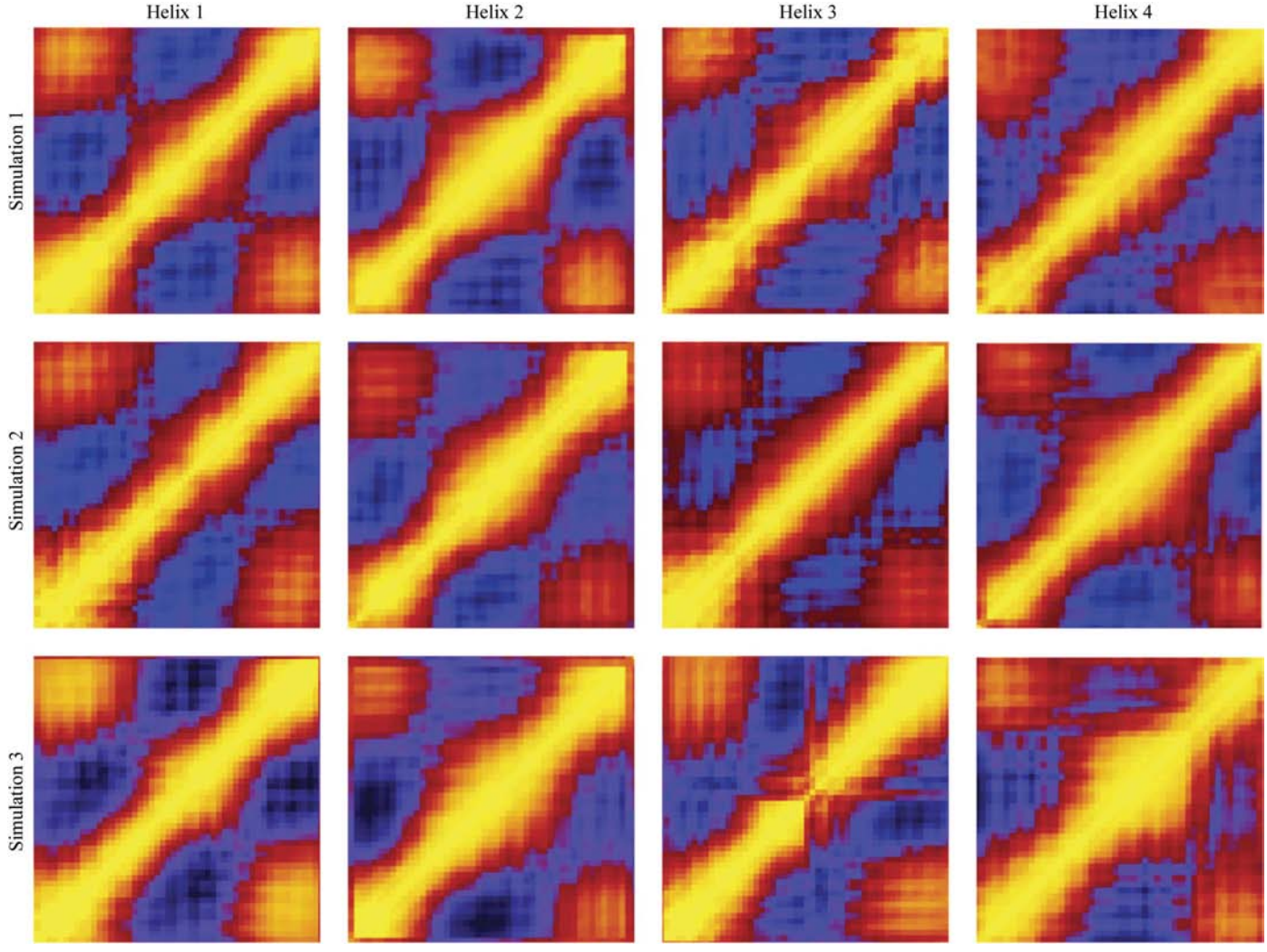

Figure 7
Pseudocolour representations of the normalized variance–covariance matrices for the four protein monomers as obtained from the three longest molecular-dynamics simulations. The colouring scheme ranges from black, through blue and red, to yellow, corresponding to values from −1.0 to 1.0.

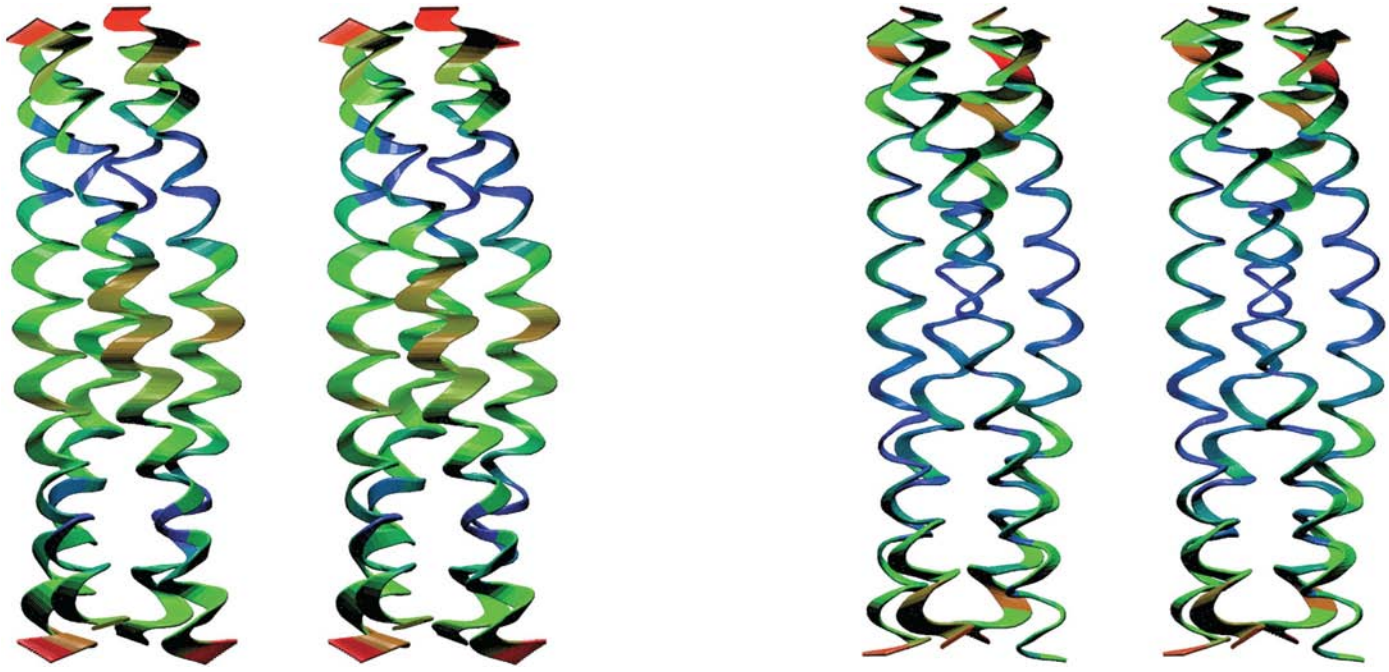

Figure 8
Stereodiagrams depicting the C^{α} motion corresponding to the two eigenvectors associated with the two largest eigenvalues. The movement of the chains is indicated through the superposition of 17 structures (for each diagram) which cover the whole range of conformations associated with each component. These 17 structures are coloured according to the value of atomic fluctuations of the C^{α} atoms from blue, through green, to red.

residues 21–34 and residues 35 to the C-terminus). The final model tested is the three-groups-per-helix model derived from the simulations as described above. The results are shown in Table 2: the conventional *R* factors decrease more-or-less monotonically with increasing number of adjustable parameters (*i.e.* number of TLS groups) as expected. This is not the case for the free *R* values, which show no appreciable difference between the first three models, but a 0.8% drop in the case of the simulation-derived TLS model. Although the reduction of the free *R* value by 0.8% may not appear to be significant, it should be noted that this is an improvement over the final statistics of a fully refined structure which already included a TLS model. More importantly, the difference between the free *R* values of the two three-groups-per-helix models appears to convincingly offer an experimental validation for the simulation-derived prediction of protein dynamics.

4. Discussion

The important conclusion from the results presented above is that, at least for the unusually thermostable protein examined, molecular-dynamics simulations appear to have matured to the point that they can be used as an analytical tool to aid not only the validation but also the refinement of crystallographically determined structures. The simulation-derived finding that the crystallographic *B* factors were seriously affected by disorder would have been difficult to identify by purely experimental (crystallographic) means. Analysis of the simulation-derived variance–covariance matrices allowed the identification of a new set of groups for TLS refinement, the application of which led to a reduction of the free *R* value of the final structure by 0.8%. Admittedly, performing computationally intensive molecular-dynamics simulations to define TLS groups is probably overkill, especially since the derived groups could have been guessed from the variation of the isotropic *B* factors (Fig. 4) or analytically determined from the application of the procedures described from Painter & Merritt (2006). The point, of course, is that if molecular dynamics indeed have enough power to make experimentally verifiable predictions, then the information content of the trajectories far exceeds the necessarily limited scope of TLS analysis and allows questions concerning the dynamics and, possibly, the function of the macromolecular component to be addressed.

I should like to thank Professor Ethan Merritt for his valuable comments and suggestions on the manuscript.

References

Amadei, A., Linssen, A. B. M. & Berendsen, H. J. C. (1993). *Proteins*, **17**, 412–425.
Brünger, A. T. (1992). *X-PLOR. Version* 3.1. Yale University, Connecticut, USA.
Brünger, A. T., Adams, P. D., Clore, G. M., DeLano, W. L., Gros, P., Grosse-Kunstleve, R. W., Jiang, J.-S., Kuszewski, J., Nilges, M., Pannu, N. S., Read, R. J., Rice, L. M., Simonson, T. & Warren, G. L. (1998). *Acta Cryst.* D**54**, 905–921.
Cheatham, T. E. III & Young, M. A. (2001). *Biopolymers*, **56**, 232–256.
Collaborative Computational Project, Number 4 (1994). *Acta Cryst.* D**50**, 760–763.

Darden, T., York, D. & Pedersen, L. (1993). *J. Chem. Phys.* **98**, 10089–10092.
García, A. E., Krumhansl, J. A. & Frauenfelder, H. (1997). *Proteins*, **29**, 153–160.
Glykos, N. M. (2006). *J. Comput. Chem.* **27**, 1765–1768.
Glykos, N. M., Papanikolau, Y., Vlassi, M., Kotsifaki, D., Cesareni, G. & Kokkinidis, M. (2006). *Biochemistry*, **45**, 10905–10919.
Grossfield, A., Feller, S. E. & Pitman, M. C. (2007). *Proteins*, **67**, 31–40.
Humphrey, W., Dalke, A. & Schulten, K. (1996). *J. Mol. Graph.* **14**, 33–38.
Ichiye, T. & Karplus, M. (1991). *Proteins*, **11**, 205–217.
Jorgensen, W. L., Chandrasekhar, J., Madura, J. D., Impey, R. W. & Klein, M. L. (1983). *J. Chem. Phys.* **79**, 926–935.
Kale, L., Skeel, R., Bhandarkar, M., Brunner, R., Gursoy, A., Krawetz, N., Phillips, J., Shinozaki, A., Varadarajan, K. & Schulten, K. (1999). *J. Comput. Phys.* **151**, 283–312.
Lange, O. F. & Grubmüller, H. (2006). *J. Phys. Chem.* **110**, 22842–22852.
Lassalle, M. W., Hinz, H.-J., Wenzel, H., Vlassi, M., Kokkinidis, M. & Cesareni, G. (1998). *J. Mol. Biol.* **27**, 987–1000.
Lindahl, E., Hess, B. & van der Spoel, D. (2001). *J. Mol. Model.* **7**, 306–317.
MacKerell, A. D. *et al.* (1998). *J. Phys. Chem. B*, **102**, 3586–3616.
McRee, D. E. (1992). *J. Mol. Graph.* **10**, 44–46.
Micu, A. M. & Smith, J. C. (1995). *Comput. Phys. Commun.* **91**, 331–338.
Merritt, E. A. & Bacon, D. J. (1997). *Methods Enzymol.* **277**, 505–524.
Murshudov, G. N., Vagin, A. A. & Dodson, E. J. (1997). *Acta Cryst.* D**53**, 240–255.
Otwinowski, Z. & Minor, W. (1997). *Methods Enzymol.* **276**, 307–326.
Painter, J. & Merritt, E. A. (2006). *Acta Cryst.* D**62**, 439–450.
Papanikolau, Y., Kotsifaki, D., Fadouloglou, V. E., Gazi, A. D., Glykos, N. M., Cesareni, G. & Kokkinidis, M. (2004). *Acta Cryst.* D**60**, 1334–1337.
Rueda, M., Ferrer-Costa, C., Meyer, T., Perez, A., Camps, J., Hospital, A., Gelpi, J. L. & Orozco, M. (2007). *Proc. Natl Acad. Sci. USA*, **104**, 796–801.
Schomaker, V. & Trueblood, K. N. (1998). *Acta Cryst.* B**54**, 507–514.
Schlick, T. (2001). *Molecular Modeling and Simulation.* New York: Springer-Verlag.
Stocker, U. & van Gunsteren, W. F. (2006). *International Tables for Crystallography*, Vol. *F*, edited by M. G. Rossmann & E. Arnold, pp. 481–488. Dordrecht: Kluwer Academic Publishers.